Direct elastic FWI updating of rock physics properties

Qi Hu, Scott Keating, and Kris Innanen

ABSTRACT

Quantitative estimation of rock physics properties is of significant interest in reservoir characterization, and most current workflows with this subject are based on amplitude variation with offset (AVO) analysis. With the expectation of more accurate results, we propose to directly estimate rock physics properties using elastic full-waveform inversion (FWI). We implement this by incorporating the rock physics model, which builds a link between elastic and rock physics properties, into the FWI workflow to reformulate the model parameterization using rock physics parameter classes. We consider three rock physics models: the Han empirical model, the Voigt-Reuss-Hill (VRH) boundary model, and the Kuster and Toksöz (KT) inclusion model. Each is used to formulate a model parameterization of porosity, clay content, and water saturation (P-C-S). We employ the truncated-Newton optimization method to update the model by iteratively minimizing the differences between synthetic and observed data. With numerical examples, our method shows considerable promise for recovering rock physics properties. It also possesses advantages over a sequential approach, which first invert for elastic attributes, then recover rock physics properties from them. We note that the Han model gives the most accurate results, whereas the KT model generally recovers the models with the largest errors. These large errors likely originate from the higher degree of nonlinearity of the KT model. The analytical radiation patterns of the P-C-S parameterization illustrate that the perturbation of water saturation has a minor effect on seismic data, this explains why water saturation is more challenging to recover compared with the porosity and clay content in our examples.

INTRODUCTION

Current seismic techniques usually go beyond inverting for elastic attributes (e.g., velocity, density, and modulus) and try to infer rock physics (or petrophysical) properties of interest, such as lithology, porosity, and fluid information (Bosch et al., 2010). The estimation of rock physics properties can be achieved either in a sequential (two-step) workflow, where seismic inversion for elastic attributes is followed by the rock physics inversion that transforms those elastic attributes to rock physics properties (Saltzer et al., 2005; Bachrach, 2006; Grana and Della Rossa, 2010; Johansen et al., 2013; Grana, 2016), or in a joint workflow, where seismic data are directly inverted for rock physics properties, often in a Bayesian formulation, with the likelihood including both rock physics and seismic forward modelings (Bosch et al., 2007; Spikes et al., 2007; Buland et al., 2008). Whether deterministic or stochastic, seismic inversions in the two workflows are commonly performed using the convolution model. The linearized amplitude variation with offset (AVO) inversion proposed by Buland and Omre (2003) represents a computationally fast and popular approach. However, AVO inversion suffers from inherent problems, in particular, it operates only with the amplitudes of reflection waves, and the migrated gathers are sensitive to errors in the velocity model (Kamath et al., 2017a). Full-waveform inversion (FWI), which employs waveforms and avoids migration-related amplitude errors, offers the likelihood of enhanced accuracy for estimating elastic and rock physics parameters.

Despite the potential of FWI as a more powerful tool for reservoir characterization, there is a paucity of literature on using it in a direct manner to estimate rock physics properties. Instead, most efforts are being directed at improving the inversion results of the elastic attributes, allowing inferences to be made on lithology or fluid information. Shi et al. (2006) design an adaptive controller to calculate suitable step length for the model iteration. This method significantly accelerates the inversion convergence, and the inverted Lamé constants yield a clear image of gas sands. Pan et al. (2018b) recommend that trade-offs between different parameter classes be evaluated using interparameter contamination kernels. These kernels explain the superiority of the velocity-density parameterization for characterizing a producing heavy oil reservoir (low Poisson's ratio) with walk-away vertical seismic profile (W-VSP) data. Prieux et al. (2013a) promote a hierarchical approach, using visco-acoustic FWI to reconstruct P-wave velocity (V_P), density, and attenuation. Several geological features, such as gas traps and soft quaternary sediments, can be interpreted with inverted density and attenuation. In their later study of visco-elastic FWI with the same field data (Prieux et al., 2013b), these geological features are more pronounced with the elastic quantities that carry a joint knowledge of V_P and V_S. In particular, the $V_\mathrm{P}/V_\mathrm{S}$ ratio allows areas saturated with gas to be discriminated, and the $V_\mathrm{P} \times V_\mathrm{S}$ quantity is representative of the lithology variations.

FWI with rock physics constraints has been viewed as a way to narrow the gap between seismic imaging and reservoir characterization (Naeini et al., 2016). Normally, the constraints are derived from facies classification using well-logs, are expressed in the form of linear relationships between elastic parameters, and are added through the regularization term to the object function (Asnaashari et al., 2013; Kamath et al., 2017a; Rocha and Sava, 2018). The key to incorporating such constraints is to estimate the spatial distribution of the facies, with repect to which the recent studies have shown promise by employing a Bayesian framework (Singh et al., 2018; Zhang et al., 2018). The facies with the maximum posterior probability at a specific grid point will determine the corresponding value in the model constraint. Despite the advantages of the facies-constrained approach for reducing the null space in multiparameter inversion, and for ensuring convergence towards a high-resolution and geologically plausible model (Kamath et al., 2017b; Zhang et al., 2017), one should weight the constraints carefully to avoid suppressing the impact of the data (Naeini et al., 2016). Besides, adding constraints is in essence a strategy for better recovering elastic attributes, from which an additional workflow is required to extract rock physics information, such as the analysis with rock physics templates calibrated with well data (Carcione and Avseth, 2015; Picotti et al., 2018) and the rock physics inversion using FWI results as input data (Dupuy et al., 2016a,b).

In this paper, we propose to directly estimate rock physics properties using isotropic-elastic FWI. The study is in part inspired by the work of Russell et al. (2011), which combines linearized AVO approximation (Aki and Richards, 2002) with poroelasticity theory (Biot, 1941; Gassmann, 1951) to generate a new model parameterization of the fluid term, shear modulus, and density, allowing us to predict fluid properties using standard AVO least-squares techniques. Likewise, we incorporate the rock physics model into FWI to formulate a model parameterization of rock physics properties, in such a way we achieve a direct update of these properties using the descent-based optimization methods (e.g., steepest descent, nonlinear conjugate gradient, and Newton-type). In real data applications, the

rock physics model adopted in the inversion generally depends on the geologic environment and has to be calibrated by well data or core measurements. For our synthetic experiments, the relations between elastic and rock physics parameters are decided by the rock physics model we choose. We consider three rock physics models: the Han empirical model, the Voigt-Reuss-Hill boundary model, and the Kuster and Toksöz (KT) inclusion model. Each is used separately to formulate a model parameterization of porosity, clay content, and water saturation. Three synthetic experiments are presented to illustrate the effectiveness of the direct approach.

THEORY AND METHODOLOGY

Isotropic-elastic full-waveform inversion

In the frequency domain, the two-dimensional elastic wave equations can be written as (Pratt, 1990)

$$\omega^2 \rho u + \frac{\partial}{\partial x}\left[(\lambda + 2\mu)\frac{\partial u}{\partial x} + \lambda\frac{\partial v}{\partial z}\right] + \frac{\partial}{\partial z}\left[\mu\left(\frac{\partial u}{\partial z} + \frac{\partial v}{\partial x}\right)\right] + f = 0,$$
$$\omega^2 \rho v + \frac{\partial}{\partial z}\left[(\lambda + 2\mu)\frac{\partial v}{\partial z} + \lambda\frac{\partial u}{\partial x}\right] + \frac{\partial}{\partial x}\left[\mu\left(\frac{\partial u}{\partial z} + \frac{\partial v}{\partial x}\right)\right] + g = 0, \tag{1}$$

where ω is the angular frequency, $\rho = \rho(x, z)$ is the density, $u = u(x, z, w)$ and $v = v(x, z, w)$ are, respectively, the horizontal and vertical displacements, $f = f(x, z, w)$ and $g = g(x, z, w)$ are the corresponding source terms, and λ and μ are the Lamé constants.

Equation 1 is discretized and solved using the finite difference equations described in Pratt (1990), which takes the form

$$\mathbf{Au} = \mathbf{f}, \tag{2}$$

where the coefficients of the impedance matrix $\mathbf{A}$ depend on the modeled frequency and the medium properties. $\mathbf{u} = (u, v)$ is the displacement vector, and $\mathbf{f} = (f, g)$ is the source vector. The perfectly matched layers (PML) method (Berenger, 1994) is used to absorb reflections from model boundaries.

FWI seeks to estimate the subsurface properties by iteratively minimizing the differences between seismic observations $\mathbf{d}_{\text{obs}}$ and the synthetic data $\mathbf{d}_{\text{syn}}$ simulated from an estimated model $\mathbf{m}$ (Pan et al., 2018a). Consider the single source/single frequency case, the associated objective function can be defined by

$$E(\mathbf{m}) = \frac{1}{2}\Delta\mathbf{d}^t\Delta\mathbf{d}^*, \tag{3}$$

where $\Delta\mathbf{d} = \mathbf{d}_{\text{obs}} - \mathbf{d}_{\text{syn}}$ is the data residual, the superscripts ^{t} and * denote the transpose and the complex conjugate, respectively.

The gradient of the ith model parameter m_i is calculated by taking the partial derivative of equation 3 with respect to m_i :

$$\nabla_{m_i}E = -\Re\left\{\left[\frac{\partial\mathbf{u}}{\partial m_i}\right]^t\Delta\mathbf{d}^*\right\}, \tag{4}$$

where $\Re$ indicates the real part operator, $\mathbf{u}$ and $\Delta\mathbf{d}$ are augmented from the receiver locations to all node points (Pratt et al., 1998). Differentiating equation 2 with repect to m_i yields the relation:

$$\mathbf{A}\frac{\partial\mathbf{u}}{\partial m_i} = -\frac{\partial\mathbf{A}}{\partial m_i}\mathbf{u}. \tag{5}$$

This shows that the partial derivative wavefield $\partial\mathbf{u}/\partial m_i$ can be computed by solving the wave equation with a virtual source $\mathbf{f} = -(\partial\mathbf{A}/\partial m_i)\mathbf{u}$. Substituting equation 5 into equation 4 gives

$$\nabla_{m_i}E = \Re\left\{\mathbf{u}^t\left[\frac{\partial\mathbf{A}}{\partial m_i}\right]^t\mathbf{A}^{-1}\Delta\mathbf{d}^*\right\}. \tag{6}$$

Using residuals as a composite source to generate the adjoint wavefield $\mathbf{A}^{-1}\Delta\mathbf{d}^*$, equation 6 allows us to efficiently calculate the gradient for all nodes, instead of solving as many forward problems (equation 5) as the number of model parameters for the virtual source. $\partial\mathbf{A}/\partial m_i$, referred to as the radiation pattern of the diffraction by m_i (Brossier et al., 2009), is often used to study parameter crosstalk and raises the issue of a suitable parameterization for multiparameter FWI.

The Newton method of optimization calculates a model update by minimizing a quadratic approximation of the objective function as seen in equation 3 (Pratt et al., 1998). The solution is characterized by

$$\mathbf{H}\delta\mathbf{m} = -\nabla_{\mathbf{m}}E, \tag{7}$$

where $\delta\mathbf{m}$ is the search direction being calculated, $\mathbf{H}$ is the Hessian operator, that is, the second derivative of the objective function with respect to model parameters. The Hessian can help in assigning the correct units to model perturbations and in mitigating parameter crosstalk, and this is the reason for its crucial importance in multiparameter FWI (Operto et al., 2013; Innanen, 2014). However, the full Newton method is normally avoided in large inverse problems due to the excessive memory and computational requirements associated with storing and inverting the Hessian (Pratt et al., 1998). Alternately, the optimization strategy employed in the paper is the truncated Gauss Newton (TGN) method (Métivier et al., 2017), which approximates the Gauss-Newton step by solving equation 7 with an iterative numerical optimization method. Instead of explicitly manipulating the Hessian, the iterative approach only requires the Hessian-vector products, which can be efficiently calculated using the adjoint state method (Plessix, 2006). Also, as a faster solver, the L-BFGS method (Nocedal, 1980) is utilized here to replace the conventional conjugate-gradient (CG) algorithm for the "inner loop" optimization problem (equation 7). The model at the kth iteration is then updated by the TGN-derived search direction $\delta\mathbf{m}_k$:

$$\mathbf{m}_{k+1} = \mathbf{m}_k + \alpha_k\delta\mathbf{m}_k, \tag{8}$$

where α_k is the step length.

Rock physics parameterizations

We denote by m_i^p the discretized parameter of class p at the spatial position indexed by i. In multiparameter FWI, the partial derivative of the impedance matrix with respect

to a new parameterization $\mathbf{q}$ (*e.g.*, $q_1 - q_2 - q_3$), can be calculated from the reference parameterization $\mathbf{p}$ (*e.g.*, $p_1 - p_2 - p_3$) using the chain rule:

$$
\begin{aligned}
\frac{\partial \mathbf{A}}{\partial m_i^{q_1}} &= \frac{\partial \mathbf{A}}{\partial m_i^{p_1}} \cdot \frac{\partial m_i^{p_1}}{\partial m_i^{q_1}} + \frac{\partial \mathbf{A}}{\partial m_i^{p_2}} \cdot \frac{\partial m_i^{p_2}}{\partial m_i^{q_1}} + \frac{\partial \mathbf{A}}{\partial m_i^{p_3}} \cdot \frac{\partial m_i^{p_3}}{\partial m_i^{q_1}}, \\
\frac{\partial \mathbf{A}}{\partial m_i^{q_2}} &= \frac{\partial \mathbf{A}}{\partial m_i^{p_1}} \cdot \frac{\partial m_i^{p_1}}{\partial m_i^{q_2}} + \frac{\partial \mathbf{A}}{\partial m_i^{p_2}} \cdot \frac{\partial m_i^{p_2}}{\partial m_i^{q_2}} + \frac{\partial \mathbf{A}}{\partial m_i^{p_3}} \cdot \frac{\partial m_i^{p_3}}{\partial m_i^{q_2}}, \\
\frac{\partial \mathbf{A}}{\partial m_i^{q_3}} &= \frac{\partial \mathbf{A}}{\partial m_i^{p_1}} \cdot \frac{\partial m_i^{p_1}}{\partial m_i^{q_3}} + \frac{\partial \mathbf{A}}{\partial m_i^{p_2}} \cdot \frac{\partial m_i^{p_2}}{\partial m_i^{q_3}} + \frac{\partial \mathbf{A}}{\partial m_i^{p_3}} \cdot \frac{\partial m_i^{p_3}}{\partial m_i^{q_3}}.
\end{aligned}
\tag{9}
$$

Equation 9 facilitates us considering a new parameterization, given that the partial derivatives of the new parameter classes with respect to the reference ones are derivable. Various elastic parameterizations (e.g., velocity-density $V_{\mathrm{P}} - V_{\mathrm{S}} - \rho$, Lamé-density $\lambda - \mu - \rho$, and modulus-density $K - G - \rho$) should be easy to deduce from one another because of the simple relationships among the elastic properties of isotropic media.

Here we consider $\mathbf{q}$ as a rock physics parameterization, namely, the model space is built with the physical properties of the rock, such as porosity, composition, and fluid saturations. To calculate the partial derivatives of the impedance matrix with respect to $\mathbf{q}$ (with $\mathbf{p}$ still being an elastic parameterization), we need to introduce a rock physics model that provides empirical or theoretical relationships between elastic and rock physics properties, to calculate $\partial m_i^{p_j} / \partial m_i^{q_k}$ ($j, k = 1, 2, 3$).

Three classic rock physics models are studied in the paper: the Han empirical model (Han, 1987), the Voigt-Reuss-Hill (VRH) boundary model (Hill, 1952), and the Kuster and Toksöz (KT) inclusion model (Kuster and Toksöz, 1974). We consider three rock physics properties that are widely used for reservoir characterization: porosity (ϕ), defined as the ratio of pore volume to the total volume of the rock; clay content (C), the ratio of clay volume to the total volume of the rock matrix; and water saturation (S_{w}), the ratio of water volume to pore volume. We use them to formulate a model parameterization of porosity, clay content, and water saturation (P-C-S), and the elastic parameterization we employ for the derivation is P- and S-wave velocities and density (D-V). Although the rock physics models are based on different theories, or even empiricism, each can express V_{P}, V_{S}, and ρ as explicit functions of ϕ, C, and S_{w}. The relations can be used to calculate the partial derivatives between the two parameterizations and ultimately, to obtain the partial derivative of the impedance matrix with respect to ϕ, C, and S_{w}.

Han empirical model

Based on the measurement of 80 well-consolidated Gulf Coast sandstones, Han (1987) found empirical regressions relating ultrasonic P-wave and S-wave velocities in km/s with porosity and clay content. A general relation can be expressed as

$$
\begin{aligned}
V_{\mathrm{P}} &= a_1 - a_2 \phi - a_3 C, \\
V_{\mathrm{S}} &= b_1 - b_2 \phi - b_3 C,
\end{aligned}
\tag{10}
$$

where a_1, a_2, a_3, b_1, b_2, and b_3 are positive constants. Assuming a solid mixture of clay and quartz, and a fluid mixture of brine and hydrocarbon (same assumptions for VRH and KT), density is computed as a weighted average of the densities of mineral and fluid components:

$$
\begin{aligned}
\rho &= (1 - \phi)\rho_m + \phi\rho_f, \\
\rho_m &= \rho_c C + \rho_q(1 - C), \\
\rho_f &= \rho_w S_w + \rho_h(1 - S_w),
\end{aligned}
\tag{11}
$$

where the subscripts m, f, c, q, w, and h indicate solid matrix, fluid phase, clay, quartz, water, and hydrocarbon (oil or gas), respectively. The partial derivatives of P-wave velocity, S-wave velocity, and density with respect to porosity, clay content, and water saturation are

$$
\begin{aligned}
\frac{\partial V_{\mathrm{P}}}{\partial \phi} &= -a_2\,, \quad \frac{\partial V_{\mathrm{P}}}{\partial C} = -a_3\,, \quad \frac{\partial V_{\mathrm{P}}}{\partial S_w} = 0\,, \\[4pt]
\frac{\partial V_{\mathrm{S}}}{\partial \phi} &= -b_2\,, \quad \frac{\partial V_{\mathrm{S}}}{\partial C} = -b_3\,, \quad \frac{\partial V_{\mathrm{S}}}{\partial S_w} = 0\,, \\[4pt]
\frac{\partial \rho}{\partial \phi} = \rho_f - \rho_m\,, \quad & \frac{\partial \rho}{\partial C} = (1 - \phi)(\rho_c - \rho_q)\,, \quad \frac{\partial \rho}{\partial S_w} = \phi(\rho_w - \rho_h)\,.
\end{aligned}
\tag{12}
$$

Voigt-Reuss-Hill (VRH) boundary model

To precisely estimate the effective elastic moduli of a mixture of grains and pores, we need to specify: 1) the individual elastic moduli of the constituents, 2) the volume fractions of the constituents, and 3) the geometric details of how the various constituents are arranged (Mavko et al., 2009). Without the details of geometry, the best we can do is to estimate the upper and lower bounds of the effective moduli.

The Voigt upper bound of the effective elastic modulus M_{V} of N constituents is

$$
M_{\mathrm{V}} = \sum_{i=1}^{N} f_i M_i,
\tag{13}
$$

where f_i and M_i are the volume fraction and the elastic modulus of the ith constituent. M can represent any modulus, such as the bulk modulus K and the shear modulus G.

The Reuss lower bound M_{R} is

$$
\frac{1}{M_{\mathrm{R}}} = \sum_{i=1}^{N} \frac{f_i}{M_i}.
\tag{14}
$$

The Voigt-Reuss-Hill average is simply the arithmetic average of the Voigt and Reuss bounds:

$$
M_{\mathrm{VRH}} = \frac{M_{\mathrm{V}} + M_{\mathrm{R}}}{2},
\tag{15}
$$

Let M_{VRH} represent the effective modulus of a saturated rock, K_{sat} or G_{sat}. Density is given by equation 11. We compute the velocities as a function of the elastic moduli and density:

$$V_{\mathrm{P}} = \sqrt{\frac{K_{\mathrm{sat}} + \frac{4}{3}G_{\mathrm{sat}}}{\rho}},$$

$$V_{\mathrm{S}} = \sqrt{\frac{G_{\mathrm{sat}}}{\rho}}. \tag{16}$$

The partial derivatives in terms of the VRH model are shown in Appendix A.

Kuster and Toksöz (KT) inclusion model

By using a long-wavelength first-order scattering theory, Kuster and Toksöz (1974) demonstrated the effects of fluid inclusions of various shapes on the seismic velocities of the rock. Assuming a single inclusion shape (or pore geometry), the following formulation can be used to compute the elastic moduli of the saturated rock (Grana, 2016):

$$(K_{\mathrm{sat}} - K_m)\frac{K_m + \frac{4}{3}G_m}{K_{\mathrm{sat}} + \frac{4}{3}G_m} = \phi(K_f - K_m)P,$$

$$(G_{\mathrm{sat}} - G_m)\frac{G_m + \xi}{G_{\mathrm{sat}} + \xi} = -\phi G_m Q, \tag{17}$$

where the subscripts sat, m, and f indicate saturated rock, solid matrix, and fluid phase, respectively. The elastic moduli of the solid matrix, K_m and G_m, is calculated using the Voigt-Reuss-Hill average (equation 15):

$$K_m = \frac{1}{2}\left[(CK_c + (1-C)K_q) + \left(\frac{1}{C/K_c + (1-C)/K_q}\right)\right],$$

$$G_m = \frac{1}{2}\left[(CG_c + (1-C)G_q) + \left(\frac{1}{C/G_c + (1-C)/G_q}\right)\right]. \tag{18}$$

Assuming a patchy saturation system, the fluid bulk modulus is given by

$$K_f = S_w K_w + (1 - S_w)K_h, \tag{19}$$

ξ is given by

$$\xi = \frac{G_m}{6}\frac{9K_m + 8G_m}{K_m + 2G_m}, \tag{20}$$

P and G are geometric factors. For spherical inclusions, P and G are given by

$$P = \frac{K_m + \frac{4}{3}G_m}{K_f + \frac{4}{3}G_m},$$

$$Q = \frac{G_m + \xi}{\xi}. \tag{21}$$

Substituting equations 20 and 21 into equation 17 yields the explicit expressions for the elastic moduli of the saturated rock:

$$K_{\text{sat}} = \frac{4K_m G_m + 3K_m K_f + 4G_m K_f \phi - 4K_m G_m \phi}{4G_m + 3K_f - 3K_f \phi + 3K_m \phi},$$

$$G_{\text{sat}} = \frac{G_m(9K_m + 8G_m)(1 - \phi)}{9K_m + 8G_m + 6(K_m + 2G_m)\phi}. \tag{22}$$

We then compute density and velocities according to equation 11 and 16. The partial derivatives in terms of the KT model are shown in Appendix B.

NUMERICAL EXPERIMENTS

Here we carry out synthetic inversion experiments using the three rock physics models. Each model helps formulate the P-C-S parameterization, upon which we can directly and simultaneously invert for porosity, clay content, and water saturation. On the other hand, when the Han's linear relations are assumed, the rock physics properties can easily be derived from the inverted P- and S-wave velocities and density that are estimated with the D-V parameterization. In this case, we compare our method with the indirect approach with respect to their performance of estimating rock physics properties.

For all experiments, we assume a rock type of gas-bearing shaley sand, where the solid phase is composed of quartz and clay, and the fluid phase composed of water and gas. The elastic properties of each constituent are listed in Table 1.

Table 1. Elastic properties of minerals and fluids.

	Bulk modulus (GPa)	Shear modulus (GPa)	Density (g/cm^3)
Quartz	37	44	2.65
Clay	21	10	2.55
Water	2.25	0	1.0
Gas	0.04	0	0.1

Inversion experiments with the Han model

We start from a toy model with an identical background porosity, clay content, and water saturation of 0.2. The model is discretized into 50 and 50 uniform mesh nodes in horizontal and vertical directions with 0.5 km in width and 0.5 km in depth. A round porosity anomaly of 0.3, a round clay content anomaly of 0.5, and a round water saturation anomaly of 0.8 are located diagonally across the model space. The initial models are homogeneous. A total of 40 sources and 100 receivers are arranged along all boundaries of the model with a regular source spacing of 50 m and a regular receiver spacing of 20 m. 10 frequency bands with 3 frequencies ranging from 2 Hz to 30 Hz per band are used. A maximum of 20 iterations for each frequency band and a maximum of 30 inner iterations are allowed in the truncated Newton approach. The Han model is used to formulate the

P-C-S parameterization and convert velocity and density to the rock physics properties in the D-V parameterization. The coefficients a_1, a_2, a_3, b_1, b_2, and b_3 in equation 10 are set to be 6, 7, 2, 4, 6, and 1.5, respectively.
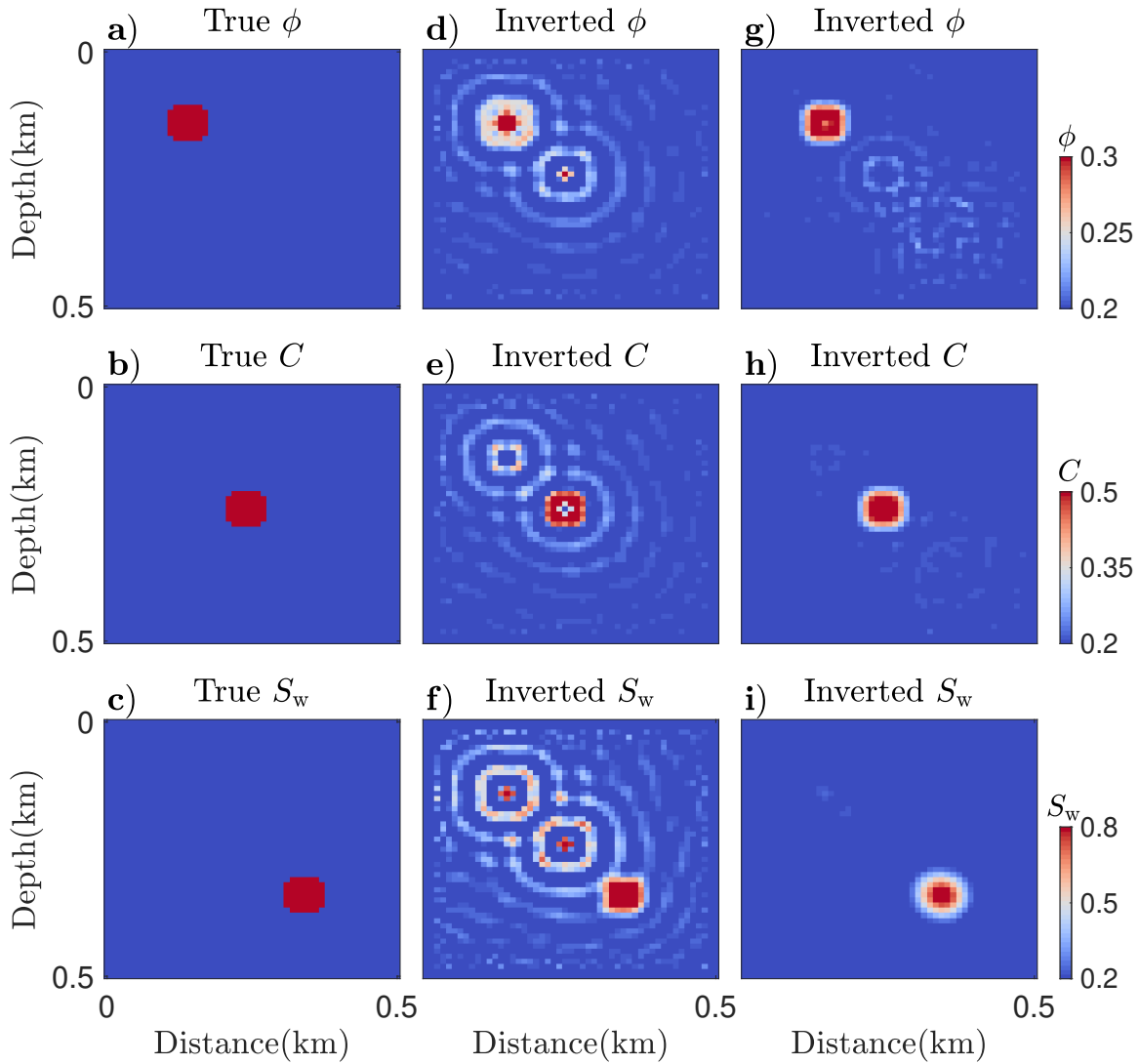

FIG. 1. (a-c) True models of ϕ, C, and S_w. The corresponding inverted models with (d-f) the D-V parameterization, and (g-i) the P-C-S parameterization.

We compare the P-C-S parameterization with the D-V parameterization in reconstructing porosity, clay content and water saturation, as shown in Figure 1, the inversion results generated by the P-C-S parameterization are highly compatible with the true models, but the results obtained with the D-V parameterization are exposed to obvious interparameter contaminations. We use the relative model error, $E = \|\mathbf{m} - \mathbf{m}_t\|/\|\mathbf{m}_0 - \mathbf{m}_t\|$, where $\mathbf{m}$, $\mathbf{m}_0$, and $\mathbf{m}_t$ represent the inverted, initial and true models, respectively, to quantify the accuracy of the inverted model. In Figure 2 we observe that the D-V parameterization actually gives a reliable estimation of velocity and density, both of whose errors are reduced rapidly and continuously as the iteration proceeds. However, the more accurate velocity and density do not necessarily result in a better estimation of rock physics properties, whose errors

can increase larger than the errors in their initial models. On the other hand, as a direct approach, the P-C-S parameterization assures a stable and efficient reduction of the model errors in the rock physics properties.
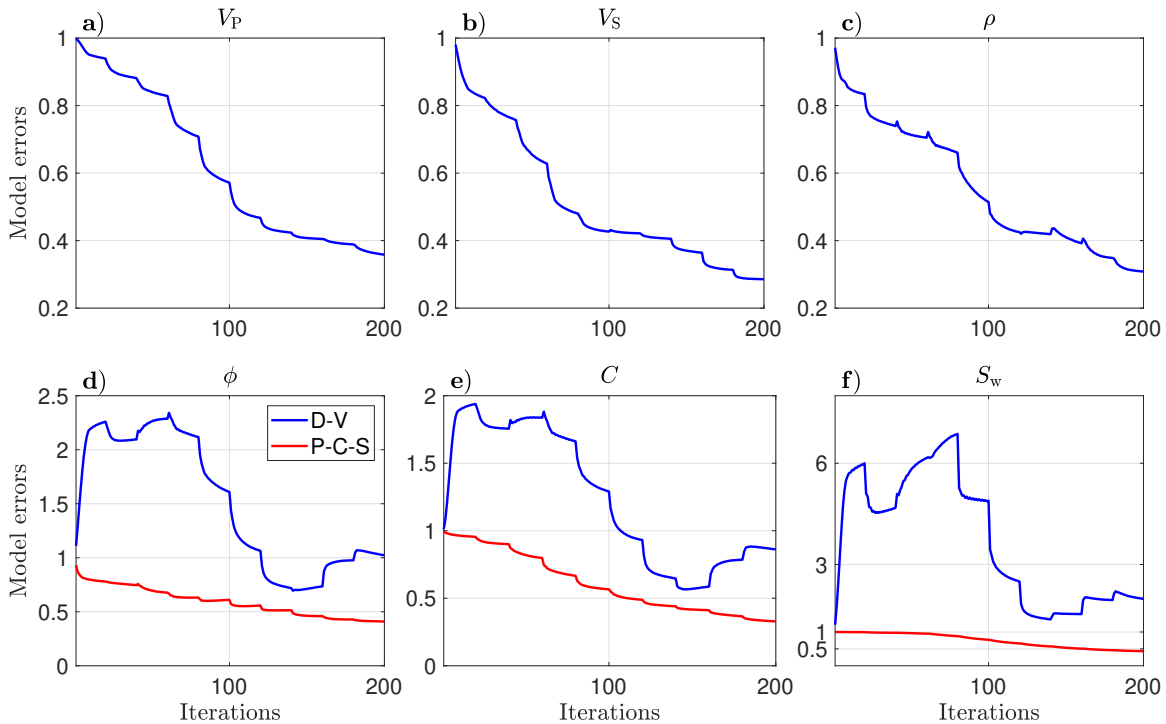

FIG. 2. (a-c) Model error reductions of V_P, V_S, and ρ in the D-V parameterization. (d-f) Comparison of the model error reductions of ϕ, C, and S_w in the D-V and P-C-S parameterizations.

We then compare the two parameterizations on a three-layer model, where a constant porosity, clay content, and water saturation are assigned to each layer (Figure 3). The initial model are generated by smoothing the true model. The model size, distribution of sources and receivers, and frequency-selection strategy are the same with those in the toy model. In Figure 4 we observe that the rock physics properties are recovered properly in the P-C-S parameterization. Even though the inverted water saturation has a slight deviation from its true amplitude, it accurately recovers the structure. Whereas in the D-V parameterization, the inverted porosity and clay content match the true models less closely, and the inverted water saturation is strongly distorted.

Still, we plot the history of model error reduction for both parameterizations, as shown in Figure 5. Despite a continuous reduction in velocity and density errors, the dramatic uphill steps can be found in the corresponding rock physics properties, especially at the beginning of the iterative process. On the other hand, the P-C-S parameterization guarantees a stable reduction of model errors and leads to more accurate inversion results.

$$\phi = 0.3, \quad C = 0.1, \quad S_{\mathrm{w}} = 0.2$$

$$\phi = 0.2, \quad C = 0.3, \quad S_{\mathrm{w}} = 0.5$$

$$\phi = 0.1, \quad C = 0.5, \quad S_{\mathrm{w}} = 0.8$$

FIG. 3. True rock physics properties of the three-layer model.
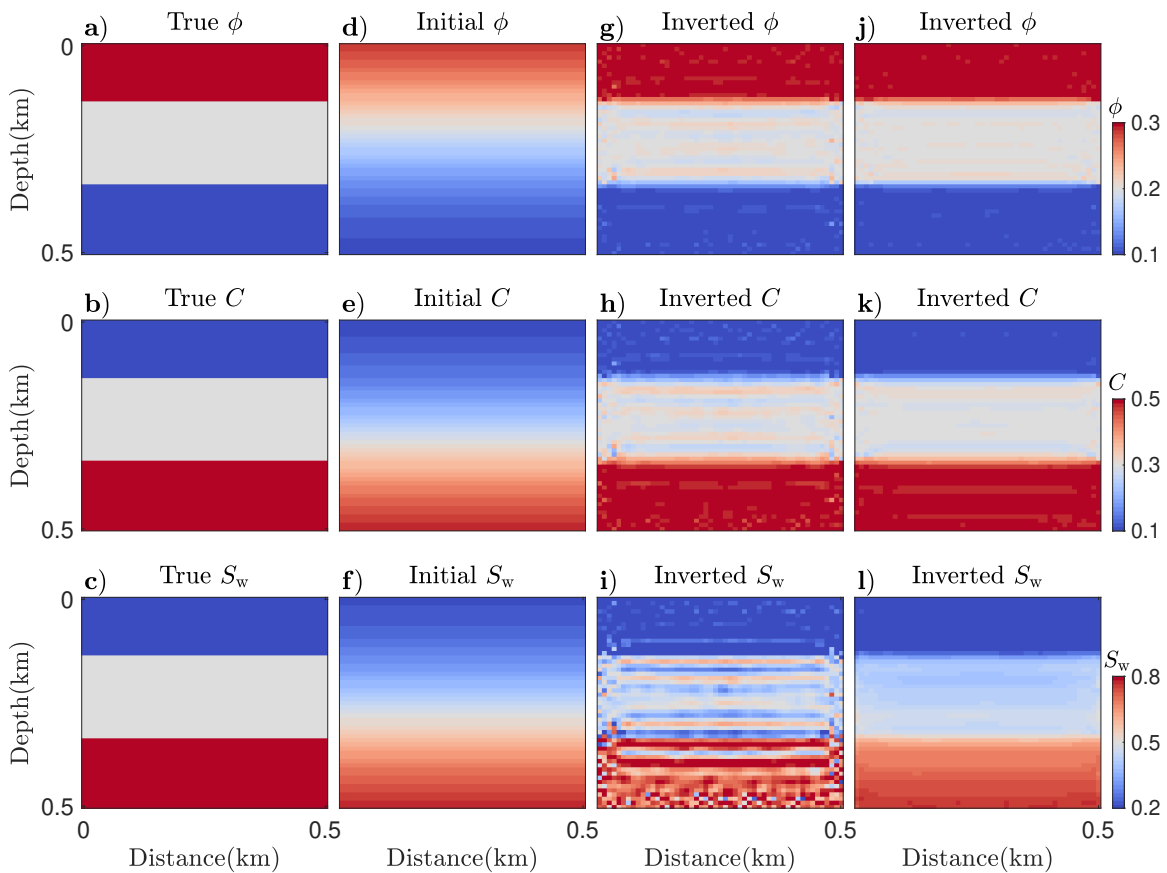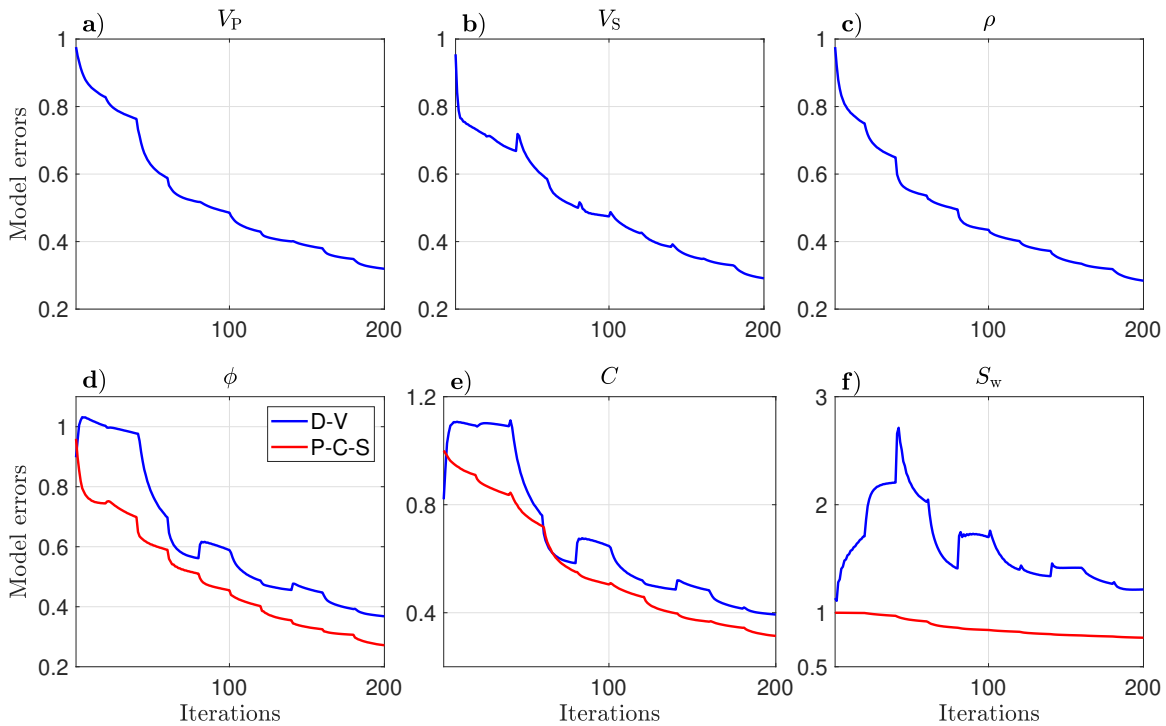

FIG. 4. (a-c) True models and (d-f) initial models of ϕ, C, and S_{w}. The corresponding inverted models with (g-i) the D-V parameterization and (j-l) the P-C-S parameterization.

FIG. 5. (a-c) Model error reductions of V_P, V_S, and ρ in the D-V parameterization. (d-f) Comparison of the model error reductions of ϕ, C, and S_w in the D-V and P-C-S parameterizations.

The derivation of porosity, clay content, and water saturation from the velocity and density are straightforward using the Han model. Nevertheless, the transformed rock physics properties are prone to large errors since they are sensitive to the errors in velocity and density. Most of the rock physics models, such as VRH and KT, are nonlinear and require complex iterative optimization algorithms to complete the transformation. This brings additional errors to the estimated rock physics properties in the indirect approach.

It is necessary to test our approach with a more plausible model that includes hydrocarbon units. We select a small part of the Marmousi2 model and adjust the model values in order to assign reasonable rock physics properties to the entire model. Figure 6a-6c shows the modified true models of P-wave velocity, S-wave velocity, and density. The model is 2 km wide and 2 km deep. Figure 6d-6f shows the transformed true models of porosity, clay content, and water saturation using the Han model. The gas sand trap, centered at a depth of 0.76 km and a distance of 0.8 km, is distinguished by a higher porosity of 0.31, a lower clay content of 0.13, and a lower water saturation of 0.34.
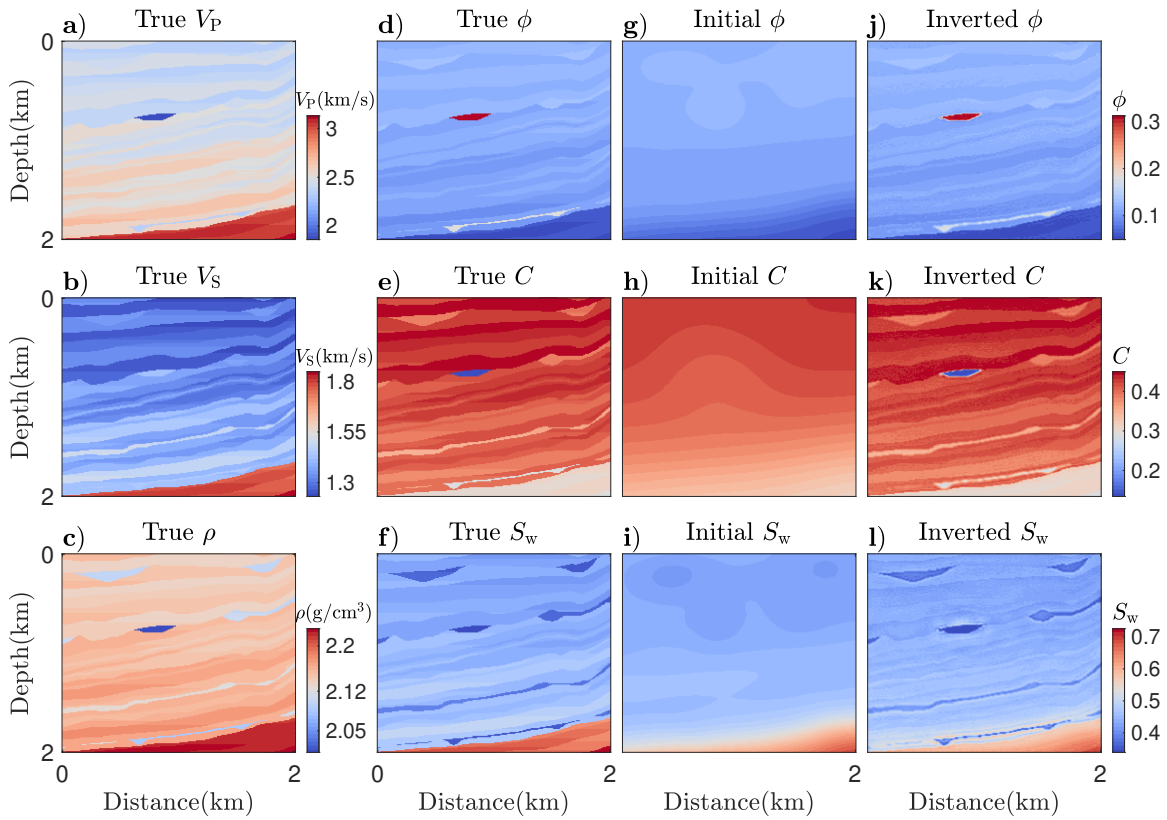
FIG. 6. (a-c) True models of V_P, V_S, and ρ. (d-f) True models, (g-i) initial models, and (j-l) the corresponding inversion results of ϕ, C, and S_w.
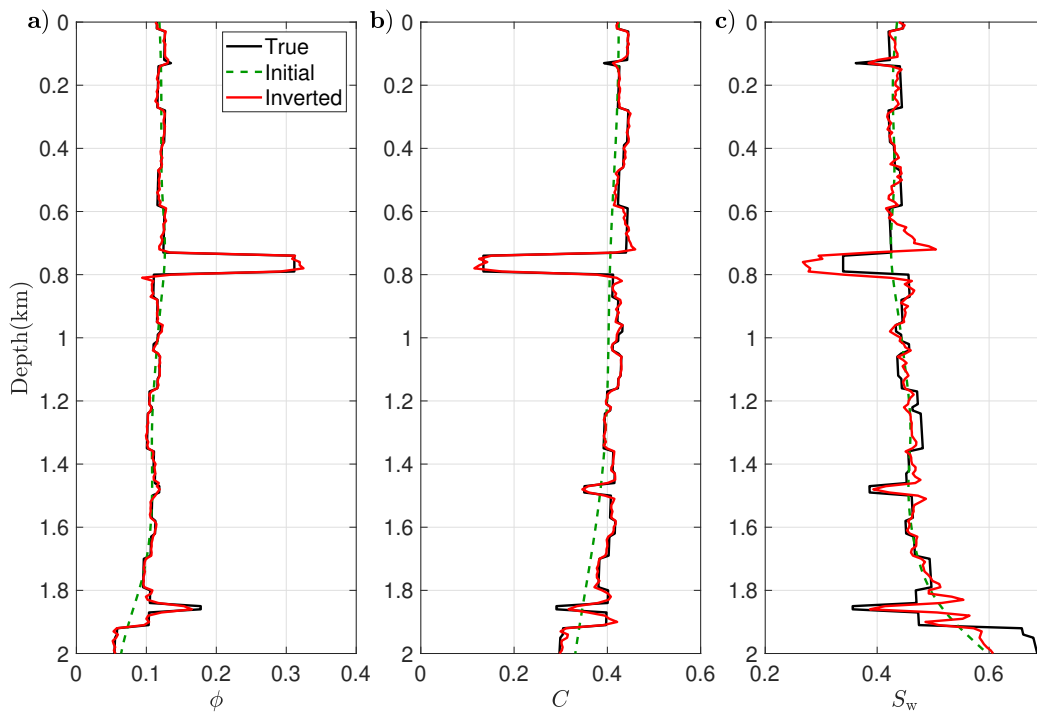

FIG. 7. Vertical profiles of the true, initial, and inverted models of a) ϕ, b) C, and c) S_w at a distance of 0.8 km

The initial models of the rock physics properties in Figure 6g-6i are smoothed versions of the true models in Figure 6d-6f. The inverted porosity, clay content, and water saturation using the P-C-S parameterization are shown in Figure 6j-6l. We observe that the inverted models almost accurately recover all layers including the gas sand trap, except that the deep structure of water saturation is not resolved sufficiently. Figure 7 shows the vertical profiles of the true, initial, and inverted models at a distance of 0.8 km, and this convinces us that the porosity and clay content are perfectly refined, whereas the inverted water saturation, although generally capturing the trend, has visible deviations from the true values in the gas trap and deep part of the model.

Inversion experiments with VRH and KT

We test the P-C-S parameterizations, formulated with the VRH model and the KT model, by applying them to the above experiments. The true and initial models of porosity, clay content, and water saturation are the same as those used for the Han model, that is to say, the three rock physics models are dealing with different true models of velocity and density in each experiment. In this section we do not intend to choose the optimal rock physics model for the P-C-S parameterization, because the selection of the rock physics model, in reality, should depend on the geologic environment and the model's ability to link the regional elastic and petrophysical variables. Instead, our purpose is to explore the adaptability of our approach under different rock physics relations.

Figures 8, 9, and 10 show the inversion results with respect to the toy model, the layered model and the modified Marmousi model, respectively, when adopting VRH and KT. We observe that in the three experiments the porosity and clay content are recovered suitably. The performance of the two rock physics models approximates each other, except for the toy model, where the results of KT apparently suffer from more crosstalk (Figure 8). The inverted water saturations, however, reconstruct to some extent the main structures but their amplitudes are weak and less comparable to the true values.
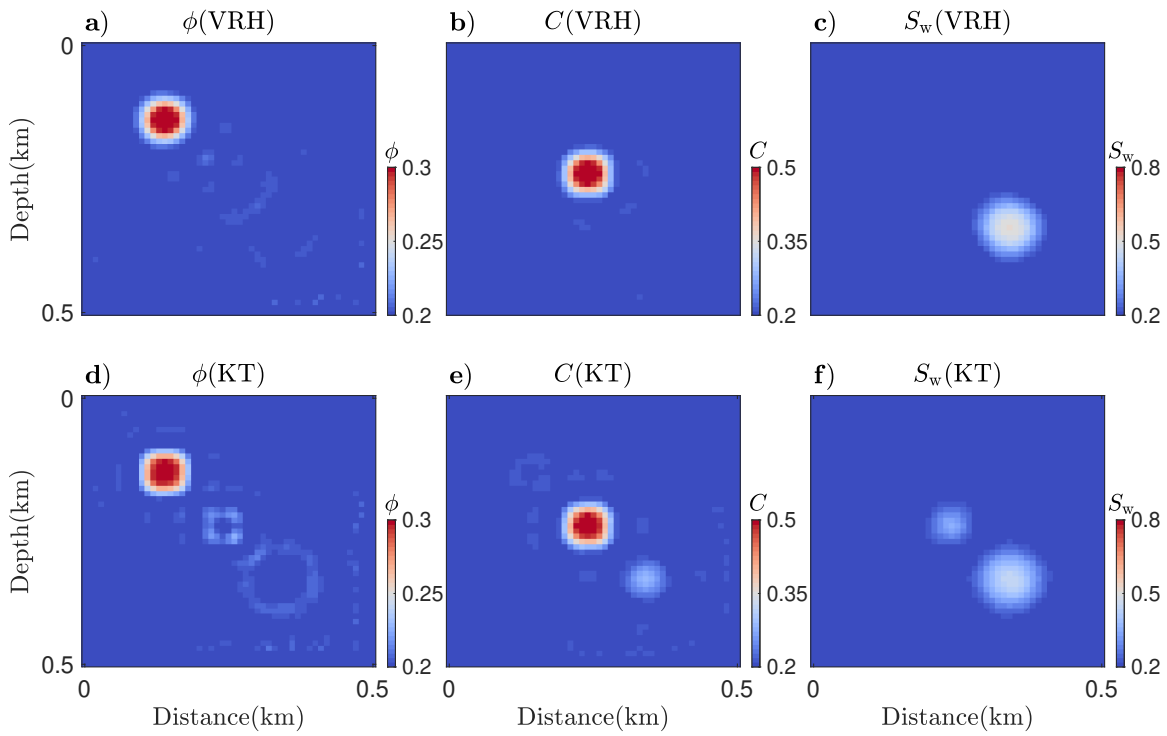
FIG. 8. Inverted models of ϕ, C, and S_{w} with (a-c) VRH and (d-f) KT.
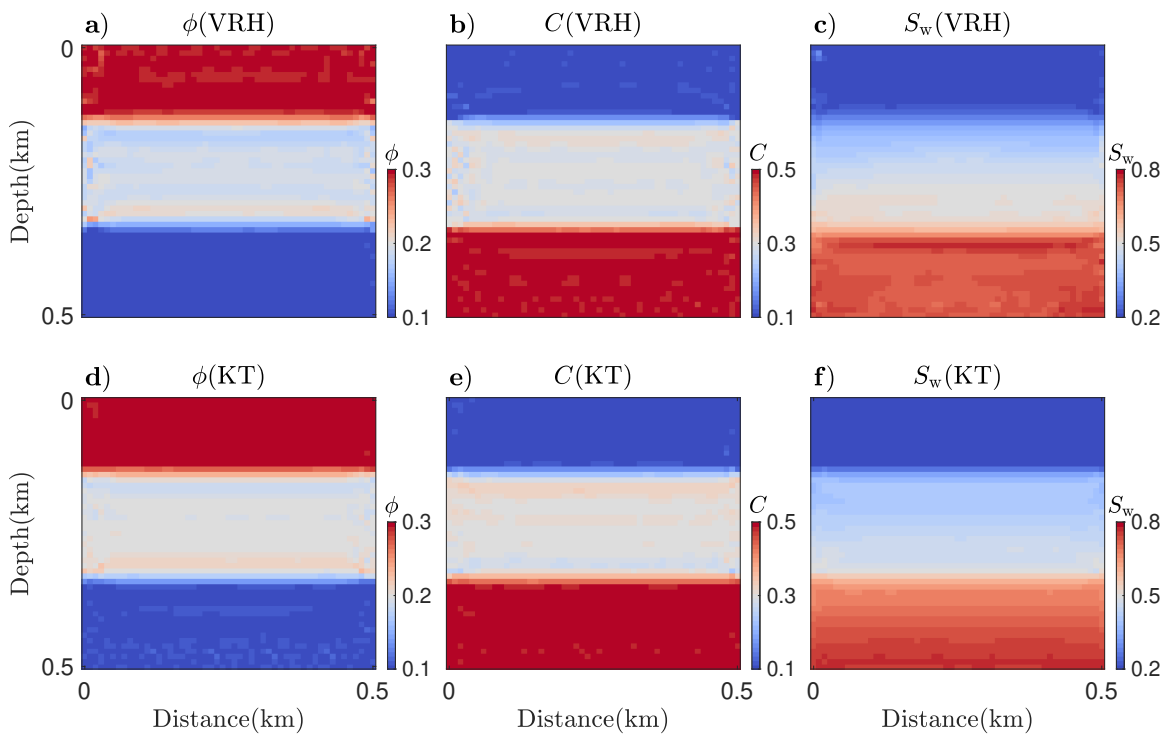

FIG. 9. Inverted models of ϕ, C, and S_{w} with (a-c) VRH and (d-f) KT.
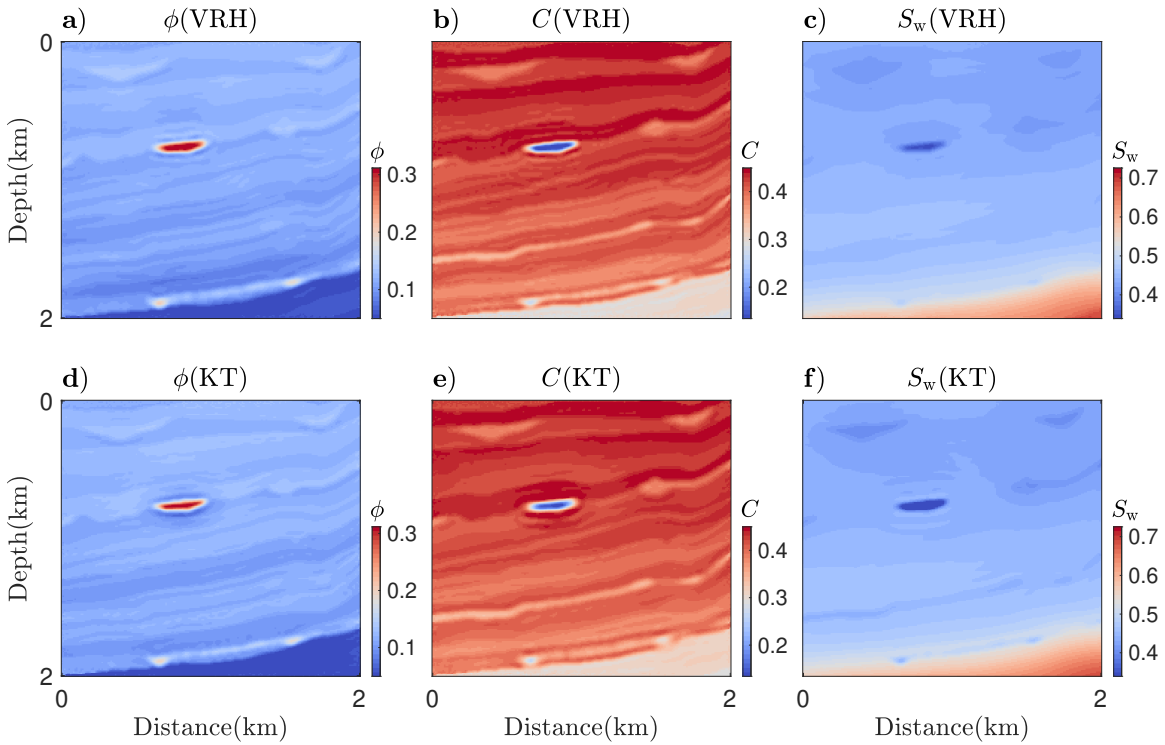
FIG. 10. Inverted models of ϕ, C, and S_{w} with (a-c) VRH and (d-f) KT.

We compare the model error reductions of the three rock physics models when they are applied to the modified Marmousi model, as shown in Figure 11. We observe that the Han model out-competes VRH and KT in reducing model errors, and this explains the lower-resolution images in Figure 10 compared to those in Figure 6. When all synthetic examples are taken into consideration, the Han model gives the most accurate estimation of porosity, clay content and water saturation, and the KT model generally recovers them with the largest errors. This likely originates from their degree of nonlinearity, as the Han model is linear, and KT is supposed to be more nonlinear than VRH, after including the latter for the computation of solid matrix.
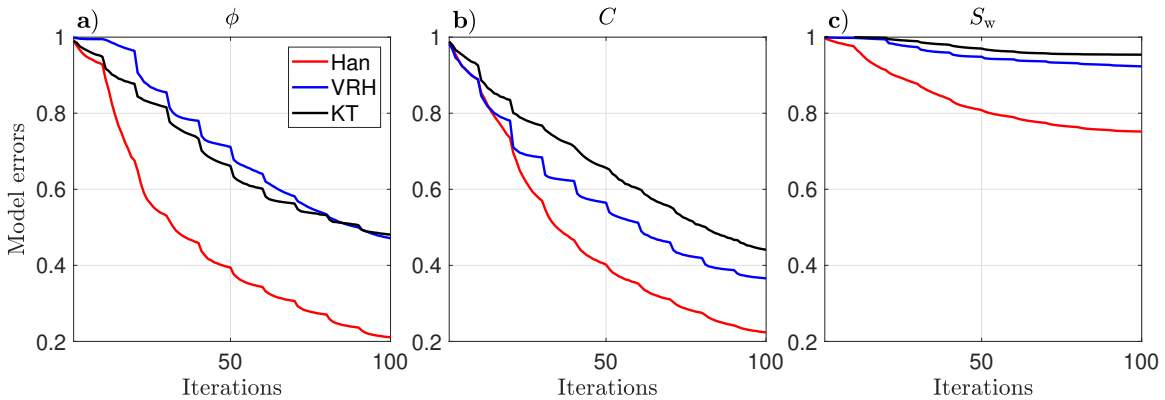

FIG. 11. Comparison of Han, VRH, and KT for reducing the model errors of a) ϕ, b) C, and c) S_{w}.

We see from different experiments that water saturation is the most difficult property to recover, this can be explained by the sensitivity analysis. Assuming a background porosity, clay content, and water saturation of 0.2, 0.5, and 0.5, we calculate the analytical scattering patterns of the P-C-S parameterization formulated with different rock physics models, as illustrated in Figure 12. Instead of analyzing the coupling effects between different parameter classes, we emphasize on the weak energy scattered by the perturbation of water saturation. When simultaneously updating the rock physics properties, as seismic data are much more sensitive to porosity and clay content, water saturation is prone to insufficient updating.
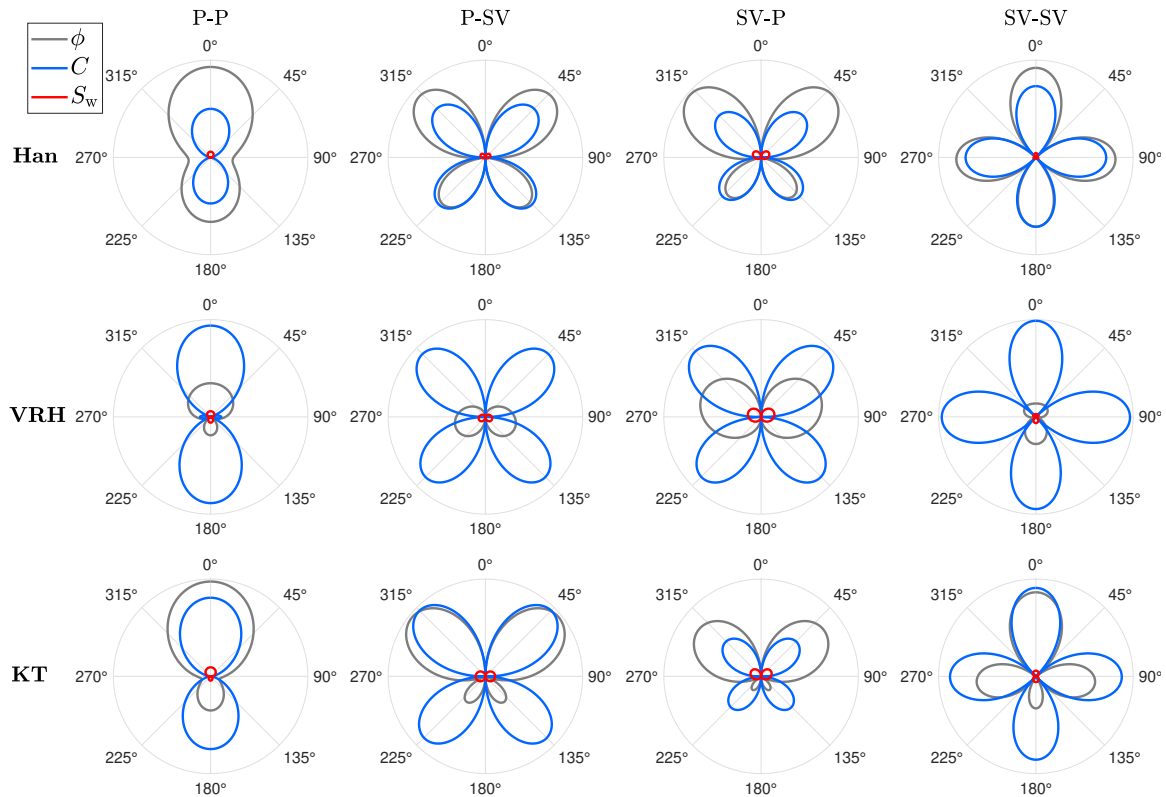

FIG. 12. Scattering patterns of ϕ, C, and S_w in the P-C-S parameterization formulated with different rock physics models.

DISCUSSION

For the experiments mentioned above, we assume an ideal situation that has recorded seismic data available in all directions. This will introduce transmission data that helps mitigate the coupling effects between different parameter classes. However, this theoretical configuration is not available in reality. We have also tested some realistic configurations (not discussed). For the most common acquisition geometry of surface-only sources and receivers, the model parameters would be less distinguished. A more powerful design could potentially be achieved by fixing vertical lines of receivers to the model. This is done to mimic a combined surface + VSP (Vertical Seismic Profile) acquisition, from which the inversion results could be largely improved compared to the pure surface acquisition, and could get close to the results from the ideal geometry.

Water saturation is very challenging to recover due to its minor contribution to seismic data. One possible solution is to use a sequential strategy, in which we need two or more inversion stages and start truly updating the water saturation at a certain stage, by using the inverted porosity and clay content from previous stages as initial models. Another approach, which is more recommended, is to replace the water saturation with a new parameter that can not only discriminate hydrocarbons, but also to which seismic data are more sensitive. The density and bulk modulus of the fluid mixture, ρ_f and K_f, as shown respectively in the Han model (equation 11) and the KT model (equation 17), can serve as the candidates. Accounting for the effects of attenuation and dispersion using visco-acoustic/elastic FWI, should provide useful information by which fluids can be discriminated (Dupuy et al., 2016a; Keating and Innanen, 2019). Various fluid factors used in the AVO inversion, like the one proposed by Russell et al. (2011), are also worth to draw lessons from.

We used three rock physics models, Han, VRH, and KT, to formulate a parameterization of porosity, clay content, and water saturation. Theoretically, once we obtain the partial derivative of an elastic attribute with respect to a rock physics property, we are able to formulate a parameterization with the rock physics property. Therefore, our approach might be promising as well when considering many other rock physics models, empirical or theoretical, based on either the effective media or the contact theory. Other rock physics properties, such as the elastic moduli of the solid matrix, dry rock, and pore fluids, or even the widely-used "aspect ratio" that describes pore geometry, can be selected as well for a direct update in FWI. We can also expand the methodology to anisotropic media, where an anisotropic rock physics model is needed to express the stiffness coefficients as a function of rock physics properties.

CONCLUSIONS

We supplement FWI with the rock physics model to achieve a direct estimation of rock physics properties based on seismic data. Three rock physics models, the Han empirical model, the VRH boundary model, and the KT inclusion model are adopted to formulate a common parameterization of porosity, clay content, and water saturation (P-C-S). The truncated-Newton optimization method, which helps mitigate parameter crosstalk without explicitly dealing with the Hessian, is used to update the rock physics properties. We carry out three synthetic experiments to examine the performance of the P-C-S parameterizations formulated with different rock physics models. In each case, the inverted porosity and clay content are highly compatible with the true models, whereas water saturation is prone to insufficient updating. This can be explained by the radiation patterns, which reveal that seismic data are not sensitive to the changes in water saturation. When we employ the Han model, our method is shown to be superior to an indirect approach, where rock physics properties are transformed from the inverted P- and S-wave velocities and density. We notice that, with respect to the three rock physics models, the Han model most accurately recovers the rock physics properties, whereas the KT model generally leads to the largest prediction errors. This may be attributed to their degree of nonlinearity.

APPENDIX A. THE VRH MODEL PARTIAL DERIVATIVES

According to equation 15, the effective bulk and shear moduli of the saturated rock are given by

$$
\begin{aligned}
K_{\text{sat}} &= \frac{K_{\text{V}} + K_{\text{R}}}{2}, \\
G_{\text{sat}} &= \frac{G_{\text{V}} + G_{\text{R}}}{2},
\end{aligned}
\tag{A.1}
$$

where

$$
K_{\text{V}} = (1 - \phi)[K_c C + K_q(1 - C)] + \phi[K_w S_w + K_h(1 - S_w)],
\tag{A.2}
$$

$$
K_{\text{R}} = 1 \bigg/ \left[\frac{(1 - \phi)C}{K_c} + \frac{(1 - \phi)(1 - C)}{K_q} + \frac{\phi S_w}{K_w} + \frac{\phi(1 - S_w)}{K_h} \right],
\tag{A.3}
$$

$$
G_{\text{V}} = (1 - \phi)[G_c C + G_q(1 - C)],
\tag{A.4}
$$

and the Reuss bound of the shear modulus $G_{\text{R}} = 0$.

Let X denote one of three rock physics properties, ϕ, C, and S_w. Substituting equations A.1, A.2, A.3, and A.4 into equation 16, we calculate the partial derivatives of P- and S-wave velocities with respect to X:

$$
\frac{\partial V_{\text{P}}}{\partial X} = \frac{1}{4\rho^2 V_{\text{P}}} \left[\left(K_{\text{V}}' + K_{\text{R}}' + \frac{4}{3}G_{\text{V}}' \right) \rho - \left(K_{\text{V}} + K_{\text{R}} + \frac{4}{3}G_{\text{V}} \right) \rho' \right],
\tag{A.5}
$$

$$
\frac{\partial V_{\text{S}}}{\partial X} = \frac{1}{4\rho^2 V_{\text{S}}} (G_{\text{V}}' \rho - G_{\text{V}} \rho'),
\tag{A.6}
$$

where the superscript $'$ stands for the derivative operator.

When X is porosity,

$$
\begin{aligned}
K_{\text{V}}' &= -K_c C - K_q(1 - C) + K_w S_w + K_h(1 - S_w), \\
K_{\text{R}}' &= K_{\text{R}}^2 \left(\frac{C}{K_c} + \frac{1 - C}{K_q} - \frac{S_w}{K_w} - \frac{1 - S_w}{K_h} \right), \\
G_{\text{V}}' &= -G_c C - G_q(1 - C), \\
\rho' &= \rho_f - \rho_m.
\end{aligned}
\tag{A.7}
$$

When X is clay content,

$$
\begin{aligned}
K_{\text{V}}' &= (1 - \phi)(K_c - K_q), \\
K_{\text{R}}' &= (1 - \phi)K_{\text{R}}^2 \left(\frac{1}{K_q} - \frac{1}{K_c} \right), \\
G_{\text{V}}' &= (1 - \phi)(G_c - G_q), \\
\rho' &= (1 - \phi)(\rho_c - \rho_q).
\end{aligned}
\tag{A.8}
$$

When X is water saturation,

$$
\begin{aligned}
K'_{\mathrm{V}} &= \phi(K_w - K_h), \\
K'_{\mathrm{R}} &= \phi K_{\mathrm{R}}^2 \left(\frac{1}{K_h} - \frac{1}{K_w} \right), \\
G'_{\mathrm{V}} &= 0, \\
\rho' &= \phi(\rho_w - \rho_h).
\end{aligned}
\tag{A.9}
$$

The partial derivatives of density with respect to ϕ, C, and S_w are the same as in equation 12.

APPENDIX B. THE KT MODEL PARTIAL DERIVATIVES

The partial derivatives of P- and S-wave velocities with respect to any rock physics property X can be written as

$$
\frac{\partial V_{\mathrm{P}}}{\partial X} = \frac{1}{2\rho^2 V_{\mathrm{P}}} \left[\left(K'_{\mathrm{sat}} + \frac{4}{3} G'_{\mathrm{sat}} \right) \rho - \left(K_{\mathrm{sat}} + \frac{4}{3} G_{\mathrm{sat}} \right) \rho' \right],
\tag{B.1}
$$

$$
\frac{\partial V_{\mathrm{S}}}{\partial X} = \frac{1}{2\rho^2 V_{\mathrm{S}}} (G'_{\mathrm{sat}} \rho - G_{\mathrm{sat}} \rho').
\tag{B.2}
$$

According to equation 22, let

$$
K_{\mathrm{sat}} = \frac{P}{Q}, \;\; G_{\mathrm{sat}} = \frac{S}{T},
\tag{B.3}
$$

so

$$
K'_{\mathrm{sat}} = \frac{P'Q - PQ'}{Q^2}, \;\; G'_{\mathrm{sat}} = \frac{S'T - ST'}{T^2},
\tag{B.4}
$$

where

$$
\begin{aligned}
P &= 4K_m G_m + 3K_m K_f + 4G_m K_f \phi - 4K_m G_m \phi, \\
Q &= 4G_m + 3K_f - 3K_f \phi + 3K_m \phi, \\
S &= G_m(9K_m + 8G_m)(1 - \phi), \\
T &= 9K_m + 8G_m + 6(K_m + 2G_m)\phi.
\end{aligned}
\tag{B.5}
$$

When X is porosity,

$$
\begin{aligned}
P' &= 4G_m K_f - 4K_m G_m, \\
Q' &= -3K_f + 3K_m, \\
S' &= -G_m(9K_m + 8G_m), \\
T' &= 6(K_m + 2G_m), \\
\rho' &= \rho_f - \rho_m.
\end{aligned}
\tag{B.6}
$$

When X is clay content,

$$
\begin{aligned}
P' &= 4(1 - \phi)(K'_m G_m + K_m G'_m) + 3K_f K'_m + 4K_f \phi G'_m, \\
Q' &= 4G'_m + 3\phi K'_m, \\
S' &= (1 - \phi)[G'_m(9K_m + 8G_m) + G_m(9K'_m + 8G'_m)], \\
T' &= 9K'_m + 8G'_m + 6\phi(K'_m + 2G'_m), \\
\rho' &= (1 - \phi)(\rho_c - \rho_q),
\end{aligned}
\tag{B.7}
$$

where

$$
\begin{aligned}
K'_m &= \frac{1}{2}\left[K_c - K_q - \left(\frac{1}{K_c} - \frac{1}{K_q}\right) \bigg/ \left(\frac{C}{K_c} + \frac{1 - C}{K_q}\right)^2 \right], \\
G'_m &= \frac{1}{2}\left[G_c - G_q - \left(\frac{1}{G_c} - \frac{1}{G_q}\right) \bigg/ \left(\frac{C}{G_c} + \frac{1 - C}{G_q}\right)^2 \right].
\end{aligned}
\tag{B.8}
$$

When X is water saturation,

$$
\begin{aligned}
P' &= (3K_m + 4G_m\phi)(K_w - K_h), \\
Q' &= 3(1 - \phi)(K_w - K_h), \\
S' &= 0, \\
T' &= 0, \\
\rho' &= \phi(\rho_w - \rho_h).
\end{aligned}
\tag{B.9}
$$

The partial derivatives of density with respect to ϕ, C, and S_w are the same as in equation 12.

ACKNOWLEDGMENTS

REFERENCES

Aki, K., and Richards, P. G., 2002, Quantitative seismology:

Asnaashari, A., Brossier, R., Garambois, S., Audebert, F., Thore, P., and Virieux, J., 2013, Regularized seismic full waveform inversion with prior model information: Geophysics, **78**, No. 2, R25–R36.

Bachrach, R., 2006, Joint estimation of porosity and saturation using stochastic rock-physics modeling: Geophysics, **71**, No. 5, O53–O63.

Berenger, J.-P., 1994, A perfectly matched layer for the absorption of electromagnetic waves: Journal of computational physics, **114**, No. 2, 185–200.

Biot, M. A., 1941, General theory of three-dimensional consolidation: Journal of applied physics, **12**, No. 2, 155–164.

Bosch, M., Cara, L., Rodrigues, J., Navarro, A., and Díaz, M., 2007, A monte carlo approach to the joint estimation of reservoir and elastic parameters from seismic amplitudes: Geophysics, **72**, No. 6, O29–O39.

Bosch, M., Mukerji, T., and Gonzalez, E. F., 2010, Seismic inversion for reservoir properties combining statistical rock physics and geostatistics: A review: Geophysics, **75**, No. 5, 75A165–75A176.

Brossier, R., Operto, S., and Virieux, J., 2009, Seismic imaging of complex onshore structures by 2d elastic frequency-domain full-waveform inversion: Geophysics, **74**, No. 6, WCC105–WCC118.

Buland, A., Kolbjørnsen, O., Hauge, R., Skjæveland, Ø., and Duffaut, K., 2008, Bayesian lithology and fluid prediction from seismic prestack data: Geophysics, **73**, No. 3, C13–C21.

Buland, A., and Omre, H., 2003, Bayesian linearized avo inversion: Geophysics, **68**, No. 1, 185–198.

Carcione, J. M., and Avseth, P., 2015, Rock-physics templates for clay-rich source rocksrpts for clay-rich source rocks: Geophysics, **80**, No. 5, D481–D500.

Dupuy, B., Garambois, S., Asnaashari, A., Balhareth, H. M., Landrø, M., Stovas, A., and Virieux, J., 2016a, Estimation of rock physics properties from seismic attributes—part 2: Applications: Geophysics, **81**, No. 4, M55–M69.

Dupuy, B., Garambois, S., and Virieux, J., 2016b, Estimation of rock physics properties from seismic attributes—part 1: Strategy and sensitivity analysis: Geophysics, **81**, No. 3, M35–M53.

Gassmann, F., 1951, Uber die elastizitat poroser medien: Vierteljahrsschrift der Naturforschenden Gesellschaft in Zurich, **96**, 1–23.

Grana, D., 2016, Bayesian linearized rock-physics inversion: Geophysics, **81**, No. 6, D625–D641.

Grana, D., and Della Rossa, E., 2010, Probabilistic petrophysical-properties estimation integrating statistical rock physics with seismic inversion: Geophysics, **75**, No. 3, O21–O37.

Han, D.-H., 1987, Effects of porosity and clay content on acoustic properties of sandstones and unconsolidated sediments: Ph.D. thesis.

Hill, R., 1952, The elastic behaviour of a crystalline aggregate: Proceedings of the Physical Society. Section A, **65**, No. 5, 349.

Innanen, K. A., 2014, Seismic avo and the inverse hessian in precritical reflection full waveform inversion: Geophysical Journal International, **199**, No. 2, 717–734.

Johansen, T. A., Jensen, E. H., Mavko, G., and Dvorkin, J., 2013, Inverse rock physics modeling for reservoir quality prediction: Geophysics, **78**, No. 2, M1–M18.

Kamath, N., Tsvankin, I., and Naeini, E. Z., 2017a, Facies-constrained fwi: Toward application to reservoir characterization: The Leading Edge, **36**, No. 11, 924–930.

Kamath, N., Tsvankin, I., and Naeini, E. Z., 2017b, Full-waveform inversion for reservoir characterization: A synthetic study, *in* SEG Technical Program Expanded Abstracts 2017, Society of Exploration Geophysicists, 3118–3122.

Keating, S., and Innanen, K. A., 2019, Parameter crosstalk and modeling errors in viscoacoustic seismic full-waveform inversion: Geophysics, **84**, No. 4, R641–R653.

Kuster, G. T., and Toksöz, M. N., 1974, Velocity and attenuation of seismic waves in two-phase media: Geophysics, **39**, No. 5, 587–618.

Mavko, G., Mukerji, T., and Dvorkin, J., 2009, The rock physics handbook: Tools for seismic analysis of porous media: Cambridge university press.

Métivier, L., Brossier, R., Operto, S., and Virieux, J., 2017, Full waveform inversion and the truncated newton method: SIAM Review, **59**, No. 1, 153–195.

Naeini, E. Z., Alkhalifah, T., Tsvankin, I., Kamath, N., and Cheng, J., 2016, Main components of full-waveform inversion for reservoir characterization: first break, **34**, No. 11, 37–48.

Nocedal, J., 1980, Updating quasi-newton matrices with limited storage: Mathematics of computation, **35**, No. 151, 773–782.

Operto, S., Gholami, Y., Prieux, V., Ribodetti, A., Brossier, R., Metivier, L., and Virieux, J., 2013, A guided tour of multiparameter full-waveform inversion with multicomponent data: From theory to practice: The Leading Edge, **32**, No. 9, 1040–1054.

Pan, W., Geng, Y., and Innanen, K. A., 2018a, Interparameter trade-off quantification and reduction in isotropic-elastic full-waveform inversion: synthetic experiments and hussar land data set application: Geophysical Journal International, **213**, No. 2, 1305–1333.

Pan, W., Innanen, K. A., and Geng, Y., 2018b, Elastic full-waveform inversion and parametrization analysis applied to walk-away vertical seismic profile data for unconventional (heavy oil) reservoir characterization: Geophysical Journal International, **213**, No. 3, 1934–1968.

Picotti, S., Carcione, J. M., and Ba, J., 2018, Rock-physics templates based on seismic q: Geophysics, **84**, No. 1, MR13–MR23.

Plessix, R.-E., 2006, A review of the adjoint-state method for computing the gradient of a functional with geophysical applications: Geophysical Journal International, **167**, No. 2, 495–503.

Pratt, R. G., 1990, Frequency-domain elastic wave modeling by finite differences: A tool for crosshole seismic imaging: Geophysics, **55**, No. 5, 626–632.

Pratt, R. G., Shin, C., and Hick, G., 1998, Gauss–newton and full newton methods in frequency–space seismic waveform inversion: Geophysical Journal International, **133**, No. 2, 341–362.

Prieux, V., Brossier, R., Operto, S., and Virieux, J., 2013a, Multiparameter full waveform inversion of multicomponent ocean-bottom-cable data from the valhall field. part 1: Imaging compressional wave speed, density and attenuation: Geophysical Journal International, **194**, No. 3, 1640–1664.

Prieux, V., Brossier, R., Operto, S., and Virieux, J., 2013b, Multiparameter full waveform inversion of multicomponent ocean-bottom-cable data from the valhall field. part 2: Imaging compressive-wave and shear-wave velocities: Geophysical Journal International, **194**, No. 3, 1665–1681.

Rocha, D., and Sava, P., 2018, Elastic reflection waveform inversion with petrophysical model constraints, *in* SEG Technical Program Expanded Abstracts 2018, Society of Exploration Geophysicists, 1203–1207.

Russell, B. H., Gray, D., and Hampson, D. P., 2011, Linearized avo and poroelasticity: Geophysics, **76**, No. 3, C19–C29.

Saltzer, R., Finn, C., and Burtz, O., 2005, Predicting v shale and porosity using cascaded seismic and rock physics inversion: The Leading Edge, **24**, No. 7, 732–736.

Shi, Y., Zhao, W., and Cao, H., 2006, Nonlinear process control of wave-equation inversion and its application in the detection of gas: Geophysics, **72**, No. 1, R9–R18.

Singh, S., Tsvankin, I., and Naeini, E. Z., 2018, Bayesian framework for elastic full-waveform inversion with facies information: The Leading Edge, **37**, No. 12, 924–931.

Spikes, K., Mukerji, T., Dvorkin, J., and Mavko, G., 2007, Probabilistic seismic inversion based on rock-physics models: Geophysics, **72**, No. 5, R87–R97.

Zhang, Z.-d., Alkhalifah, T., and Naeini, E. Z., 2017, Multiparameter elastic full waveform inversion with facies constraints, *in* SEG Technical Program Expanded Abstracts 2017, Society of Exploration Geophysicists, 1551–1555.

Zhang, Z.-d., Alkhalifah, T., Naeini, E. Z., and Sun, B., 2018, Multiparameter elastic full waveform inversion with facies-based constraints: Geophysical Journal International, **213**, No. 3, 2112–2127.